Metals and Materials International
https://doi.org/10.1007/s12540-024-01798-3

A Novel Form "Bubble Microstructure" in LPBF and Investigation of Its Mechanical Strength on TPMS-Gyroid

Cemal İrfan Çalışkan[1] · **Gökhan Özer**[2] · **Hamaid Mahmood Khan**[2]

Received: 6 May 2024 / Accepted: 25 August 2024

Abstract
In our previous research within the scope of process parameters change, the innovative 30 µm synchronous scanning strategy (SSS) in the Laser Powder Bed Fusion production system and the effect of this scanning strategy on industrial gears were discussed in the microstructure examination of industrial gears produced with this scanning strategy. It was observed that the Additive Manufacturing (AM) traditional melt pool form changed, and the strength increased by approx. 23%. In this article, carried out in the second stage, a new microstructure in the form of bubbles obtained with this new synchronous scanning strategy, discussed in depth with laboratory research, is defined as "Bubble Microstructure." This new microstructure definition, which constitutes the innovative side of the study, is in addition to the 30 µm SSS research that was discussed in the first phase of the study; 40 µm SSS production and research carried out at this stage are detailed within the scope of tensile tests in ASTM-E8 standard, detailed microstructure examinations in OM (Optic Microscope) and SEM (Scanning Electron Microscope), EDX, XRD analyzes and the mechanical strength effect of this microstructure on the Triple Periotic Minimal Surfaces geometry. This new SSS approach is considered promising in industrial areas where innovative geometries can be produced with AM, weight-reduced designs using topology optimization, and DfAM (Design for Additive Manufacturing) are used.

Keywords Additive manufacturing · Laser powder bed fusion · Synchronous scanning strategy · Process parameters · Triply periotic minimal surfaces

1 Introduction

Selective laser melting (SLM) is an increasingly popular additive manufacturing method for producing three-dimensional objects from individual powder particles. This technique involves a high-powered laser guided by a preset CAD model to traverse over a bed of powder, melting and bonding the particles together to create a solid structure (Hamaid Mahmood [16, 21]). The process doesn't just rely on the intensity of the laser; several other parameters, including hatching distance, layer thickness, beam diameter, and laser scanning speed, are carefully adjusted. This ensures that the molten material effectively integrates with the previously solidified layers, resulting in a robust and well-integrated structure [15, 17, 18].

Products created using the selective laser melting (SLM) process demonstrate impressive durability, longevity, and environmentally responsible and economically essential attributes for sustainable metal production [8, 23]. SLM offers unlimited geometric possibilities, freedom in design, and versatility in material choice, which broadens its application across various industrial sectors. Furthermore, SLM excels in the precise design and fabrication of innovative materials in micro-areas, opening up new opportunities for in situ alloying [5, 11, 15, 17, 18].

AlSi10Mg is a popular alloy for SLM processes, favored for its rapid solidification rate and high yield strength, which is significantly higher than that of its cast form [3, 10, 14, 24]. This alloy is extensively adopted in automotive and aerospace applications due to its performance characteristics. It boasts a yield strength of approximately 300 MPa, facilitated by its microstructure, which includes a network of α-Al (FCC)/Si eutectic located within the inter-dendritic areas

✉ Cemal İrfan Çalışkan
cemalirfancaliskan@gmail.com; ccaliskan@itu.edu.tr

[1] Department of Industrial Design, Istanbul Technical University, Istanbul, Türkiye

[2] Fatih Sultan Mehmet Vakif University, Aluteam, Beyoglu, Istanbul, Türkiye

Published online: 02 November 2024

of a supersaturated α-Al matrix [1, 6, 13]. Additionally, the formation of semi-coherent Mg2Si particles enhances its strength by acting as barriers to dislocation movement under stress ([12].

Numerous studies have concentrated on the parametric optimization of SLM for the near-net-shape fabrication of AlSi10Mg components. Enhancements in component strength, for example, have been linked to increasing laser power and decreasing scanning speed, which contributes to the formation of a more homogeneous melt pool and reduces pore formation [15, 17, 18, 20]. Decreasing the hatching distance has also improved the bonding between scanning tracks and subsequent layers [19]. Moreover, a layer thickness of about 30 µm has been identified in several studies as optimal for ensuring successful melt pool penetration into preceding layers, thereby facilitating strong interlayer bonding [2]. The literature also indicates that excessive heat input into a melt pool due to poorly optimized laser parameters can significantly reduce the strength of metal structures. Several review literature is available to present the overview of the influence of laser processing parameters on the performance of metal strength and microstructure [9, 15–18]. Thus, it is crucial to carefully optimize laser parameters to achieve optimal process efficiency and product quality.

This study introduces a novel microstructure, identified as the "Bubble Structure" and created through a synchronous scanning strategy that diverges from the conventional melt pool shape typically observed in the SLM processing of AlSi10Mg. This new scanning approach has facilitated a 25% increase in strength compared to traditional methods. Our previous research employed a synchronous 30 µm process parameter to achieve thermal equilibrium between the design and the production platform [4]. The innovative approach transformed the traditional oval-shaped melt pool into a bubble-like structure, leading to substantial material strength improvements and enhanced weight reduction and topology optimization capabilities using the SSS methodology [4]. This research presents an innovation to the literature by introducing a novel microstructure defined as a "Bubble Structure." The conditions under which this new microstructure is formed are revealed in detail by metallographic tests. The definition of this new microstructure refers to the new microform referred to as SSS, which is found by the synchronized scanning strategy in the LPBF production process parameters. The research is a study in which this microstructure is defined, and its mechanical strength effect is discussed in the case of 40 µm layer thickness and on the gyroid form. Suppose it is necessary to give information about the scanning strategy expressed as SSS. In that case, it refers to the production strategy realized by equalizing the hatch distance, layer thickness, and stripe width parameters using the same value. With SSS, X (hatch distance), Y (stripe width), and Z (layer thickness) are aimed to provide more balanced heat distribution in the layers with a value of 30 µm or 40 µm, which are determined in common in all three parameters and directions. In this research, the effect of SSS with 40 µm on mechanical properties is fully revealed, and "Bubble Structure" is introduced to the literature. Due to the increased research on the production of cellular forms with AM in recent years, it is thought that gyroid and similar innovative forms will be mentioned and used more in future industries. For this reason, gyroid compression tests were added to the research within the scope of the mechanical strength effect of this new microstructure developed with SSS on cellular forms.

This research extensively analyzed the mechanical strength and microstructural characteristics using several methods. Tensile tests conducted according to ASTM-E8 standards, alongside in-depth microstructural examinations using Optical Microscopy (OM) and Scanning Electron Microscopy (SEM), as well as Energy Dispersive X-ray Spectroscopy (EDX) and X-ray Diffraction (XRD) analyses, were pivotal in evaluating the performance. Additionally, the impact of the newly developed microstructure was assessed through compression tests on gyroid geometries derived from the Triply Periodic Minimal Surface (TPMS) group, showcasing one of the bio-inspired designs achievable with additive manufacturing. The study also included a comparative analysis of the mechanical and microstructural performances using the current synchronous scanning strategy (SSS) parameters set at 30 µm and 40 µm with the standard parameter set, providing a comprehensive evaluation of these modified processing parameters.

2 Experimental

2.1 Methods and Materials

The present study involved an in-depth analysis using four samples to compare and evaluate the proposed approach effectively. Table 1 displays the layer thickness selections for the samples under investigation, allowing for a detailed examination of how varying layer thicknesses impact the study's overall results.

In this study, we employed standard laser processing parameters recommended by the EOS SLM machine manufacturer and our newly proposed approach. Sample m1 uses the standard laser processing parameters for AlSi10Mg material with a 30 µm layer thickness, a setup previously noted in several studies [15, 22]. The proposed approach includes the SSS sample from our prior research [4], denoted here as sample m2, for comparative analysis.

Table 1 Four production definitions were used in the research

m1 (AlSi10Mg)	m2 (AlSi10Mg)	m3 (AlSi10Mg)	m4 (AlSi10Mg)
30 µm standard	30 µm bubble	40 µm standard	40 µm bubble

Additionally, samples m3 and m4 were created with a layer thickness of 40 µm to explore the effects of increased layer thickness. Sample m3 adheres to the standard processing conditions and features the traditional melt pool configuration, making it identical to sample m1 except for the difference in layer thickness. Conversely, sample m4 employs the SSS approach but with a 40 µm layer thickness, where the distinct bubble structure is also achieved, offering a unique point of comparison against the more conventional configurations.

In this study, sample m4 represents the implementation of a 40 µm layer thickness using the Synchronous Scanning Strategy (SSS), a method discussed for the first time in this article and not previously covered in the literature. The standard and synchronized process parameters used in all samples (m1, m2, m3, m4) produced as part of this research are detailed in Table 2. Table 2 highlights several parameters, such as hatch distance, layer thickness, and stripe width. Unlike the traditional X-Rotated scanning strategy, the SSS adopted an X–Y scanning approach, another modification to optimize the production process. All samples were manufactured using the aluminum alloy AlSi10Mg, widely utilized in AM-LPBF processes. The specific chemical composition of this alloy is provided in Table 3.

2.2 Bubble Microstructure Metallography Laboratory Studies

Four types of rectangular prism structures measuring 12 × 12 × 5 mm were fabricated for microstructural analysis using parameter sets m1, m2, m3, and m4 on the EOS-M290 AM-LPBF system. Following production, these samples underwent surface preparation in the metallography lab, which included sequential sanding with silicon carbide abrasives at grit sizes of 320, 600, 800, 1000, and 2500 µm.

After sanding, the samples were polished using Keller's etch, which is a mixture of 96.22% water, 2.59% nitric acid, 0.64% hydrochloric acid, and 0.55% hydrofluoric acid to analyze the microstructural features of the alloy. The surfaces of the prepared samples were then examined under an optical microscope. The images captured from these examinations are presented in Fig. 1.

According to the microstructural images in Fig. 1, the differences between the standard and novel scanning strategies are visible across various parameter sets. Figure 1a displays the traditional melt pool form observed in sample m1, produced using standard parameters with a layer thickness of 30 µm. Figure 1b highlights the novel 30 µm bubble structure microstructure achieved in sample m2, showcasing the synchronous scanning strategy (SSS) effects at this layer thickness.

Figure 1c, on the other hand, shows the traditional microstructure form in sample m3, produced using the 40 µm standard parameter set, maintaining the conventional melt pool configuration but at an increased layer thickness. Lastly, Fig. 1d presents the 40 µm bubble structure in sample m4. This new microstructure, evaluated for the first time in this study, illustrates how modifications in the SSS, combined with an increased layer thickness, can influence the development of the microstructure, potentially affecting mechanical properties and performance.

SEM was employed to closely observe the samples for a more detailed examination of the microstructural features, as shown in Fig. 2.

Table 2 Process parameters of the productions made in this research

	m1(std.)	m2(bubble)	m3(std.)	m4(bubble)
laser power	370 W	370 W	370 W	370 W
laser scan speed	1300 mm/s	1300 mm/s	1300 mm/s	1300 mm/s
Hatch distance	0.19 mm	30 µm	0.19 mm	40 µm
layer thickness	30 µm	30 µm	40 µm	40 µm
beam offset	0.02 mm	0.02 mm	0.02 mm	0.02 mm
laser intensity	49.932 J/mm^3	316.239 J/mm^3	49.932 J/mm^3	316.239 J/mm^3
Scanning strategy	X-Rotated	X–Y	X-Rotated	X–Y
temperature	30 °C (building platform)	30 °C (building platform)	30 °C (building platform)	30 °C (building platform)
Strip width	7 mm	30 µm	7 mm	40 µm
laser type	Yb (Ytterbium) fibre laser	Yb (Ytterbium) fibre laser	Yb (Ytterbium) fibre laser	Yb (Ytterbium) fibre laser
atmosphere	Argon	Argon	Argon	Argon

Table 3 Chemical composition of AlSi10Mg material [7]

%	Al	Cu	Fe	Mg	Mn	Si	Ti	Zn	Zr
AlSi10Mg	balance	< 0.05	< 0.55	0.25–0.45	< 0.45	9.0–1.0	< 0.15	< 0.10	–

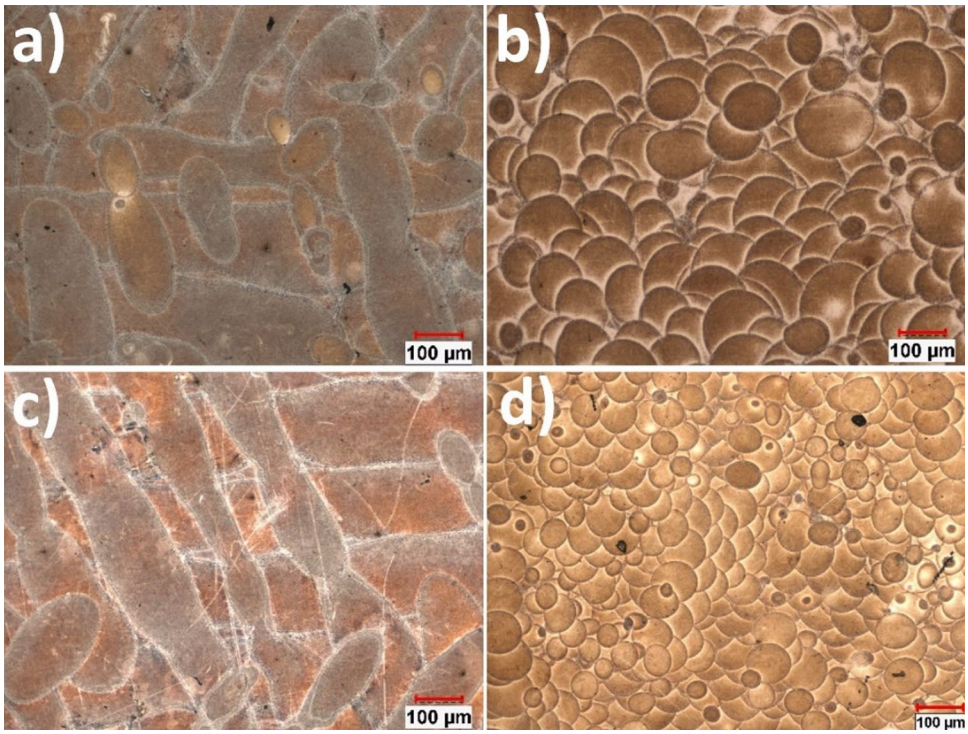

Fig. 1 **a** m1, **b** m2, **c** m3, and **d** m4, optic microstructure of the samples (top surfaces)

Upon detailed examination of the AlSi10Mg samples produced using the parameters for m2 and m4, a distinctive spherical microstructure was observed, which had not been previously documented in the literature. This unique formation is named the "bubble microstructure" due to its spherical, bubble-like appearance.

As observed, the traditional laser tracks typically visible in the as-built microstructure (samples m1 and m3) had vanished in samples m2 and m4. Instead, a new microstructure

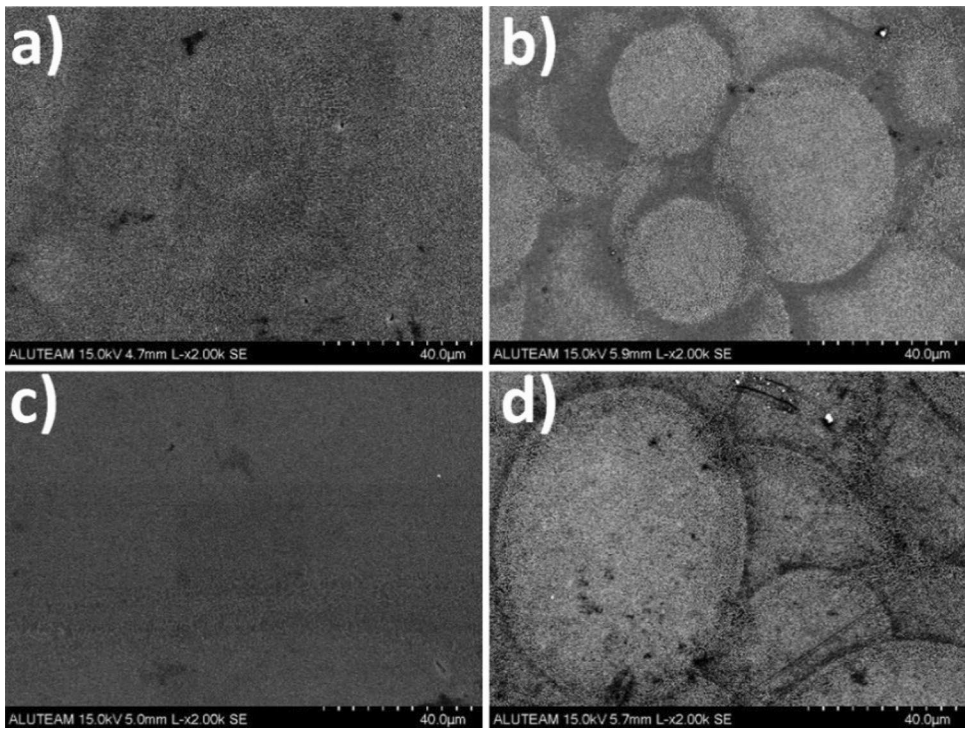

Fig. 2 **a** m1, **b** m2, **c** m3, and **d** m4 SEM microstructure of the samples (top surfaces)

composed entirely of these spherical "bubbles" emerged. This transformation is depicted in Fig. 3, which illustrates how the synchronous scanning strategy fundamentally alters the material's morphology at a microstructural level.

Upon conducting the EDX analysis on the samples, particularly examining the melt pool border regions within the bubble structure, it was noted that the cellular silicon structure, typically visible within the matrix, had disappeared between the bubbles. Moreover, the EDX analysis further revealed that these regions between the bubbles were depleted in silicon, as demonstrated in Fig. 4. This silicon depletion highlights a significant alteration in the chemical distribution within the bubble structure's microenvironment compared to the traditional microstructures.

In the XRD analysis of the samples, distinct Al and Si peaks were detected, as illustrated in Fig. 5. Notably, no precipitates were observed in the diffraction patterns. However, the analysis showed a significant change in the intensity of the Si peaks, especially in the 30-µm bubble sample (m2). The increased intensity of these Si peaks suggests enhanced solubility of silicon within the aluminum matrix, which is particularly noticeable around the bubble areas.

Porosity analysis was performed on Zeiss Smartzoom5 with Zen core 3.5 program. Porosity measurements were performed using a coloring technique.

The porosity ratios of the samples are given in Fig. 6 and Table 4.

When the porosity values are analyzed, the lowest porosity belongs to M1 and M2 samples produced with the newly developed SSS technique. The porosity values of the samples produced with the traditional screening strategy were relatively high.

2.3 Tensile Test and Mechanical Strength on TPMS-Gyroid

Following the comprehensive microstructural analysis, mechanical evaluations were conducted to assess the performance of the newly identified bubble microstructure. This involved conducting tensile tests to measure mechanical

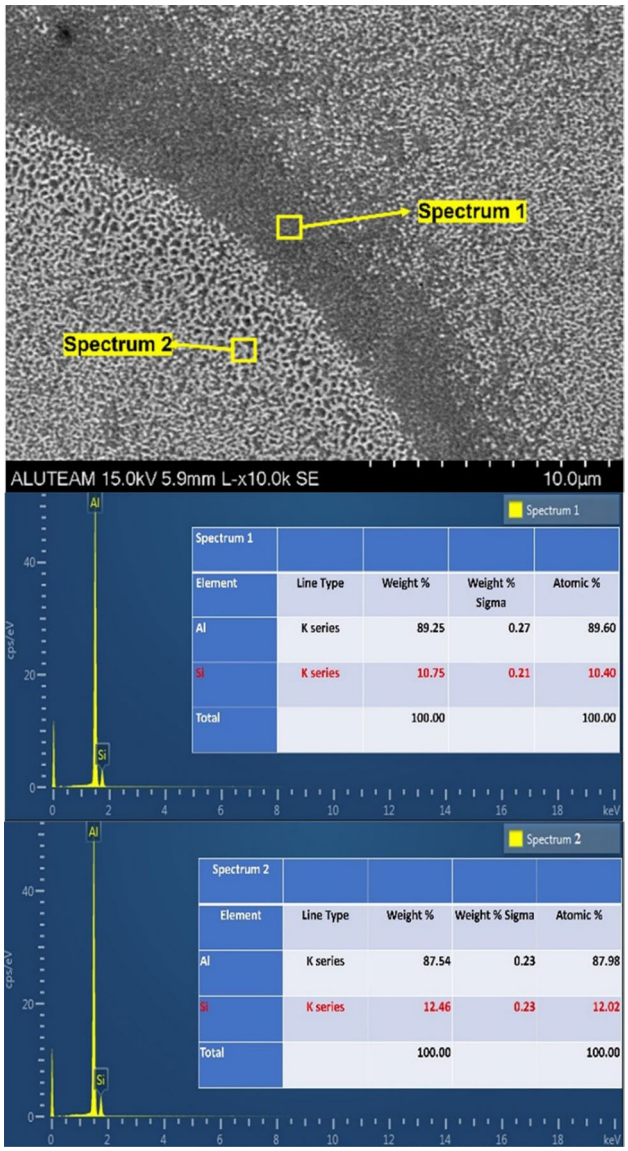

Fig. 4 EDX analysis

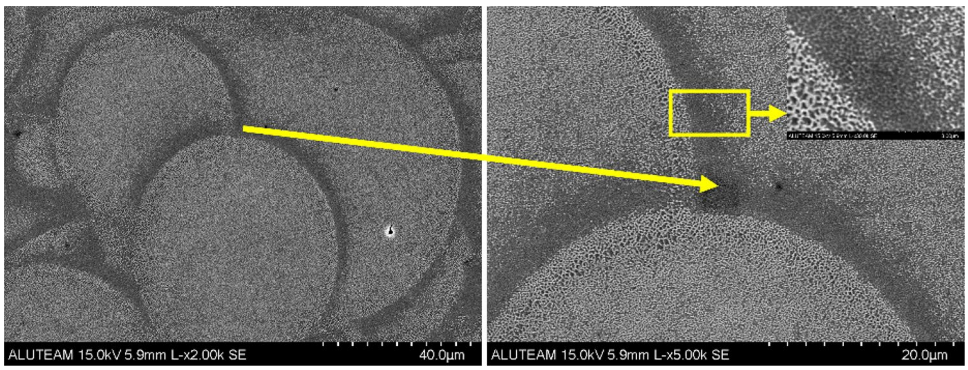

Fig. 3 Detailed view of the bubble microstructure

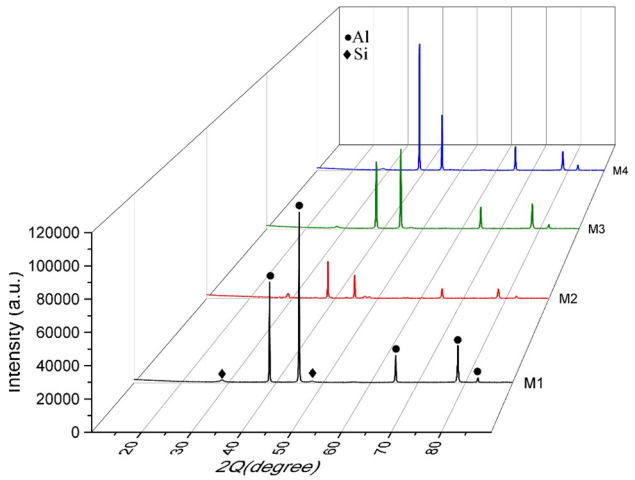

Fig.5 XRD analysis

strength and examining mechanical behavior in innovative cellular forms. Samples corresponding to each parameter set m1, m2, m3, and m4 were produced for these tests.

For each parameter set, four different types of tensile test samples were fabricated by ASTM-E8 standards. Four samples featuring gyroid geometry within infilled rectangular prisms were also created for each set to be tested in compression tests. This approach allowed for the direct comparison of mechanical properties across the different microstructures and processing conditions. These test samples are shown in Fig. 7.

Table 4 Porosity ratios of samples

	m1(std.)	m2(bubble)	m3(std.)	m4(bubble)
Porosity (%)	0.985	0.123	0.841	0.480

Tensile and compression tests were rigorously conducted using the ALSA (100 kN) compression test system, with each test being repeated four times to ensure reliability and consistency in the data. The strength values obtained from these tests are detailed in the study's results section. Additionally, a camera closely monitored and recorded the compression test process specifically applied to the gyroid geometry. This allowed for an accurate visual of how the geometry deformed at various compression rates. The detailed observations of these deformations under different stress levels have been systematically tabulated and presented in the results section.

3 Results and Discussion

The microstructural investigation of the samples processed using standard techniques and the novel SSS revealed significant differences in their microstructural formations. Notably, the traditional melt pool forms characterized by long scan tracks, typically vulnerable to impurities and exhibiting pronounced microstructural variations at the borders, have been replaced by a bubble-type microstructure in the

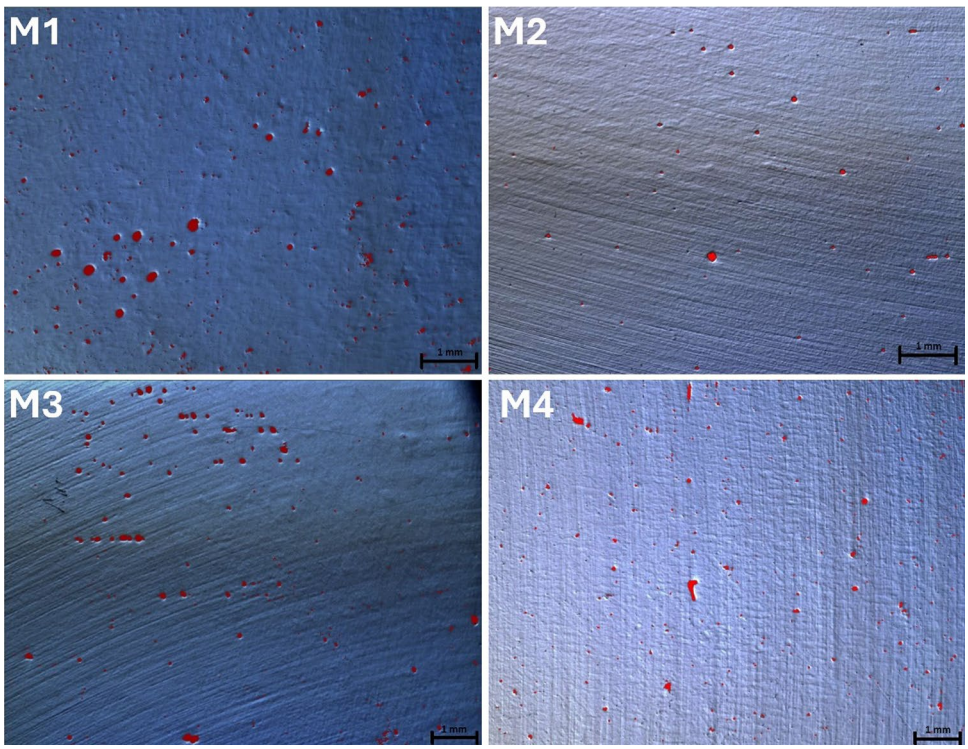

Fig. 6 Porosity ratios of the samples

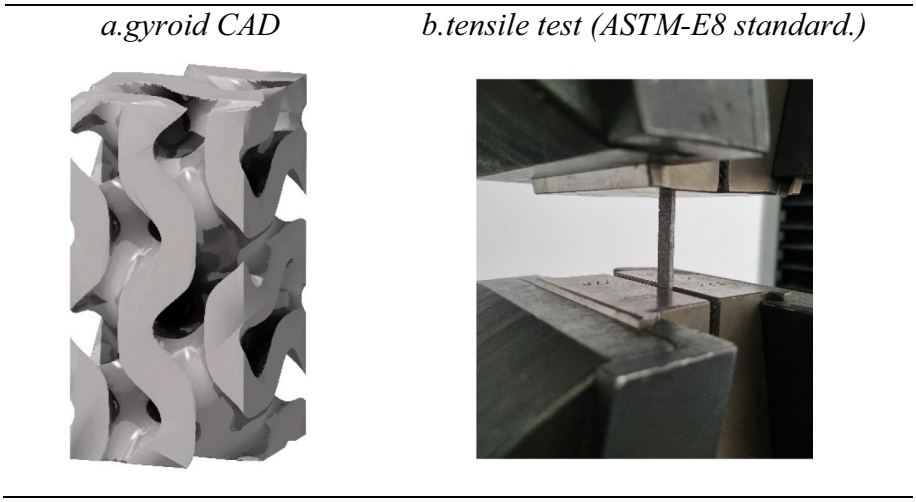

Fig. 7 **a** Gyroid geometry with dimensions of 10 × 10 × 20mm used in compression tests, **b**Tensile test sample and test stage in ASTM-E8 standard

samples processed with the SSS (m2 and m4). This deviation from the traditional long melt pool tracks, commonly seen as potential weak points for crack initiation and propagation under mechanical stress or even as sites for electrochemical variations under adverse conditions, marks a significant improvement. The bubble-type microstructure lacks these long tracks, a change that is prominently visible in the figures provided.

Furthermore, the OM and SEM analyses still show melt pool boundaries but a smaller melt pool shape. The application of the SSS likely induces a higher energy input into the melt pool due to the chosen processing parameters, especially the 30 µm hatching strategy. This energy input results in high heating of the melt pool and rapid solidification, resulting in microstructure characterized by increased strength because of the higher solubility of Si within the melt pool. This increased Si solubility could potentially improve the mechanical properties of AlSi10Mg, contributing to better performance in applications requiring high strength and durability.

The increased solubility of silicon is understood to enhance the mechanical properties of AlSi10Mg alloys. This is due to silicon's ability to form a robust Al-Si solid solution and generate small precipitates that block the movement of dislocations, thereby strengthening the material. Additionally, the rapid cooling characteristic of the SLM process aids in achieving high silicon solubility, which facilitates the development of a refined microstructure with uniformly dispersed silicon particles. This finer microstructure contributes to higher yield strength and greater hardness. Further analysis of the mechanical properties of newly proposed samples indicated a similar trend of improved performance.

Table 5 presents the average strength values derived from tension tests. This data shows that the strength measured in the m2 tensile tests, which utilized a bubble microstructure, is approximately 28% higher than that of the m1 tests

Table 5 Tensile test results

m1 (MPa)	m2 (MPa)	m3 (MPa)	m4 (MPa)
320	410	317	391

Table 6 Compression test results applied to gyroid geometry

m1 (kN)	m2 (kN)	m3 (kN)	m4 (kN)
115	130	110	127

conducted at the same layer thickness. Furthermore, when comparing the m3 and m4 specimens, tested at a 40 µm layer thickness, the average strength in the bubble structure sample showed a roughly 23% increase. Metallographic testing and analysis have indicated that this enhancement in mechanical strength is likely due to the transformation of the laser tracks in the microstructure into a bubble microstructure.

In the study, the outcomes from compression tests exploring the impact of mechanical strength on gyroid geometry are presented in Table 6. The gyroid structure was modeled for these tests like a rectangular prism measuring 10 × 10 × 20 mm. The specifics of the gyroid modeling included a wall thickness of 2 mm, a cell distance of 2 mm, and a fill rate of 61.7%. Each test was repeated at least three times to ensure the reliability of the results. Strain strain graphs of tension test specimens are given in Fig. 8. As shown, bubble-type structures displayed better performance compared to the standard models.

According to the data in Table 6, there is an approximately 13% increase in mechanical strength from sample *m1* to *m2*. The strength difference between the gyroid samples m3 and m4 is about 15%. These results, evident from both compression and tension tests,

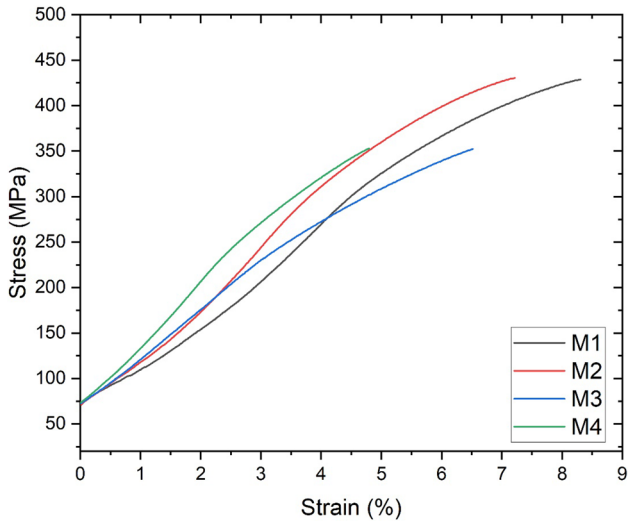

Fig. 8 Stress–strain graph of tension test samples of all variations

indicate a notable improvement in strength for the bubble-type geometry compared to traditional manufacturing approaches across both tension and gyroid samples. Given the consistent geometry across samples, the rise in strength in each instance can largely be attributed to the alterations in the microstructural formation of the bubble-type structure. This significant enhancement in strength is crucial for enhancing the overall structural and mechanical performance in practical applications.

For a comprehensive analysis aimed at interpreting the impact of bubble microstructure on mechanical strength, video footage from the compression tests was edited to synchronize with the exact timings of each compression event. The deformation states of each model were analyzed at intervals of 1, 3, 5, and 10 mm. Table 7 displays the photographic documentation of these deformations, captured at these specified intervals, to provide visual insights into how the bubble microstructure responds to compressive stress.

During the compression tests for the gyroid samples m1 and m3, produced using standard parameters, a clear progression of geometric distortion is evident right after 1 mm of compression. By the end of the compression test at 10 mm of distortion, these samples can be observed breaking apart completely. In contrast, the samples with bubble morphology (m2 and m4), designed using the SSS strategy, showed significantly better resistance to the compression tests than their traditional counterparts. Sample m2 demonstrated the most robust performance among all the tested specimens, highlighting the effectiveness of the bubble morphology in enhancing mechanical resilience.

4 Conclusions

This study examines the mechanical and microstructural performance of SLM components fabricated using a standard and a novel synchronous scanning strategy (SSS). The results revealed that components produced with SSS exhibited a distinctive bubble-like microstructure, differing from the semi-elliptical forms typically seen in standard LPBF processes. This bubble microstructure, along with an increased solubility of silicon within the alloy, led to a stronger Al-Si solid solution and finer precipitates, thus enhancing the material's overall strength. Furthermore, these microstructural changes have significantly improved the materials' resistance to deformation and rupture under stress compared to those with conventional microstructures.

The mechanical testing of the samples showed that those with the bubble microstructure, particularly samples m2 and m4, demonstrated markedly higher strength and better performance during compression tests than the traditional microstructure samples (m1 and m3). Sample m2, in particular, exhibited exceptional resistance to deformation, outperforming all other specimens. Implementing the SSS strategy not only facilitated the creation of bubble microstructures but also eliminated the formation of long melt pool tracks, which are typically prone to impurities and structural weaknesses. The likely increase in energy input during processing contributed to higher silicon solubility, which was critical in strengthening the resultant alloy. As a result of this study, it can be said that the SSS technique is also effective in reducing porosity.

This new microstructure introduced by the SSS strategy represents a promising avenue for further research. Future studies should focus on thoroughly characterizing this microstructure through corrosion, impact, and wear studies to understand its properties and potential applications fully. Additionally, investigating how this microstructure performs in innovative lattice geometries, designs optimized through topology optimization, and complex internal geometries producible via additive manufacturing will be crucial for advancing the technology and expanding its application scope in various industries.

Table 7 Deformation conditions at 1, 3, 5, and 10 mm were taken from compression test video recordings of gyroid geometry

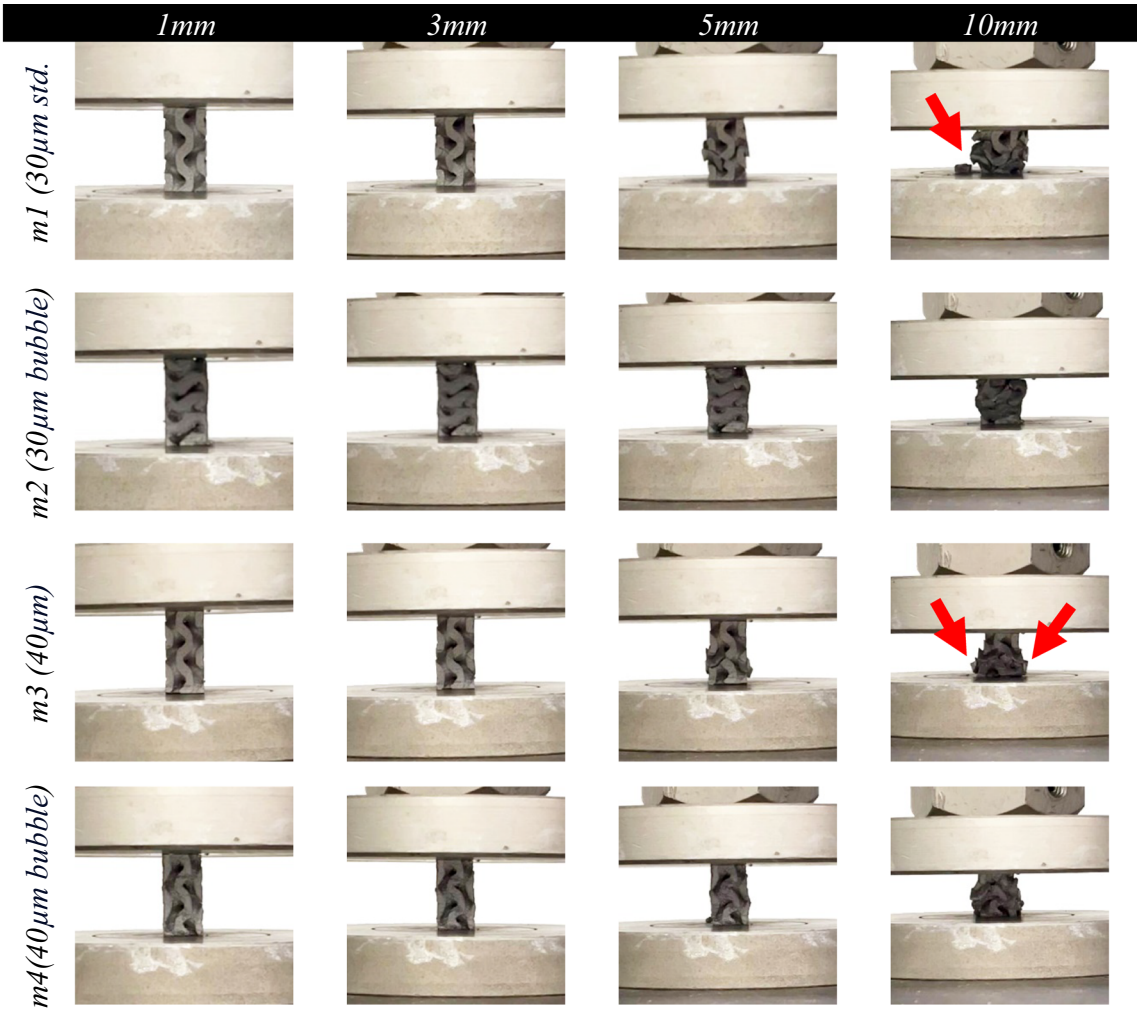

Acknowledgements Istanbul Technical University Scientific Research Projects Coordination Department, ITU Scientific Research Project ID:45766, has financially supported innovative concept proposals and design studies of the research. In addition, laboratory studies of this research were supported within the scope of the "Aluteam: Joint Research Center Project for the Digital Transformation of the Aluminum Industry," a European Union Project (IPA) supported by the Ministry of Industry and Technology.

Authors contributions Cemal İrfan Çalışkan, innovative concept proposal, design and table studies, authorship; Gökhan Özer laboratory studies, authorship, and table studies; Hamaid Mahmood Khan, authorship and literature research.

Data Availability The authors confirm that the data and material supporting the findings of this work are available within the article.

Declarations

Conflict of interest The authors have no competing interests or conflicts of interest to declare relevant to this article's contents.

Ethical Approval The article follows the guidelines of the Committee on Publication Ethics (COPE) and involves no studies on human or animal subjects.

References

1. H. Asgari, C. Baxter, K. Hosseinkhani, M. Mohammadi, On microstructure and mechanical properties of additively manufactured AlSi10Mg_200C using recycled powder. Mater. Sci. Eng. A **707**, 148–158 (2017). https://doi.org/10.1016/j.msea.2017.09.041
2. S. Cacace, Q. Semeraro, Influence of the atomization medium on the properties of stainless steel SLM parts. Addit. Manuf. **36**, 101509 (2020). https://doi.org/10.1016/j.addma.2020.101509
3. F. Calignano, D. Manfredi, E.P. Ambrosio, L. Iuliano, P. Fino, Influence of process parameters on surface roughness of aluminum parts produced by DMLS. Int. J. Adv. Manuf. Technol. **67**(9–12), 2743–2751 (2013). https://doi.org/10.1007/s00170-012-4688-9

4. C.İ Çalışkan, A novel synchronous scanning strategy in laser powder bed fusion and effect on mechanical properties of industrial gears. Int. J. Adv. Manuf. Technol. **128**(5–6), 2459–2467 (2023)
5. C.İ Çalışkan, G. Özer, E. Koç, U.S. Sarıtaş, C.F. Yıldız, Ö.Y. Çiçek, Efficiency research of conformal channel geometries produced by additive manufacturing in plastic injection mold cores (Inserts) used in automotive industry. 3D Print. Addit. Manuf. **10**, 213–225 (2021). https://doi.org/10.1089/3dp.2021.0062
6. B. Chen, S.K. Moon, X. Yao, G. Bi, J. Shen, J. Umeda, K. Kondoh, Strength and strain hardening of a selective laser melted AlSi10Mg alloy. Scr. Mater. **141**, 45–49 (2017). https://doi.org/10.1016/j.scriptamat.2017.07.025
7. EOS. (2022). *EOS Aluminium AlSi10Mg Material Data Sheet*
8. D. Faidel, D. Jonas, G. Natour, W. Behr, Investigation of the selective laser melting process with molybdenum powder. Addit. Manuf. **8**, 88–94 (2015). https://doi.org/10.1016/j.addma.2015.09.002
9. J. Gardan. (2017). Additive manufacturing technologies: State of the art and trends. in *Additive Manufacturing Handbook: Product Development for the Defense Industry,* ed. by A.B. Badiru, V.V. Valencia, D. Liu Vol. 54 (CRC Press, United ststes, 2017), pp. 149–168
10. V. Hammond, M. Schuch, M. Bleckmann, The influence of a process interruption on tensile properties of AlSi10Mg samples produced by selective laser melting. Rapid Prototyp. J. **25**, 1445–1452 (2019). https://doi.org/10.1108/RPJ-04-2018-0105
11. Y. Hou, H. Su, H. Zhang, X. Wang, C. Wang, Fabricating Homogeneous FeCoCrNi High-Entropy Alloys via SLM In Situ Alloying. Metals **11**(6), 942 (2021). https://doi.org/10.3390/met11060942
12. K. Kempen, L. Thijs, E. Yasa, M. Badrossamay, W. Verheecke, J.P. Kruth, Process optimization and micostructural analysis for selective laser melting of AlSi10Mg, in *2011 International Solid Freeform Fabrication Symposium* (University of Texas, Austin, 2011), pp. 484–495. https://doi.org/10.26153/tsw/15310
13. K. Kempen, L. Thijs, J. Van Humbeeck, J.P. Kruth, Mechanical properties of AlSi10Mg produced by selective laser melting. Phys. Procedia **39**, 439–446 (2012). https://doi.org/10.1016/j.phpro.2012.10.059
14. H.M. Khan, M.H. Dirikolu, E. Koç, Parameters optimization for horizontally built circular profiles: numerical and experimental investigation. Optik **174**, 521–529 (2018). https://doi.org/10.1016/j.ijleo.2018.08.095
15. H.M. Khan, C.İ Çalışkan, M.E. Bulduk, The novel hybrid lattice structure approach fabricated by laser powder bed fusion and mechanical properties comparison. 3D Print. Addit. Manuf. **10**, 1371–1380 (2022). https://doi.org/10.1089/3dp.2022.0224
16. H.M. Khan, Y. Karabulut, O. Kitay, Y. Kaynak, I.S. Jawahir, Influence of the post-processing operations on surface integrity of metal components produced by laser powder bed fusion additive manufacturing: a review. Mach. Sci. Technol. **25**(1), 118–176 (2021). https://doi.org/10.1080/10910344.2020.1855649
17. H.M. Khan, G. Özer, M.S. Yilmaz, E. Koc, Corrosion of additively manufactured metallic components: a review. Arab. J. Sci. Eng. **47**(1), 5465–5490 (2022). https://doi.org/10.1007/s13369-021-06481-y
18. H.M. Khan, S. Waqar, E. Koç, Evolution of temperature and residual stress behavior in selective laser melting of 316L stainless steel across a cooling channel. Rapid Prototy. J. **28**(7), 1272–1283 (2022). https://doi.org/10.1108/RPJ-09-2021-0237
19. E. Liverani, S. Toschi, L. Ceschini, A. Fortunato, Effect of selective laser melting (SLM) process parameters on microstructure and mechanical properties of 316L austenitic stainless steel. J. Mater. Process. Technol. **249**, 255–263 (2017). https://doi.org/10.1016/j.jmatprotec.2017.05.042
20. T. Maconachie, M. Leary, B. Lozanovski, X. Zhang, M. Qian, O. Faruque, M. Brandt, SLM lattice structures: properties, performance, applications and challenges. Mater. Des. **183**, 108137 (2019). https://doi.org/10.1016/j.matdes.2019.108137
21. M. Majeed, H.M. Khan, G. Wheatley, R. Situ, Influence of post-processing on additively manufactured lattice structures. J. Braz. Soc. Mech. Sci. Eng. **44**(9), 389 (2022). https://doi.org/10.1007/s40430-022-03703-8
22. G. Tarakçı, H.M. Khan, M.S. Yılmaz, G. Özer, Effect of building orientations and heat treatments on AlSi10Mg alloy fabricated by selective laser melting: microstructure evolution, mechanical properties, fracture mechanism and corrosion behavior. Rapid Prototyp. J. **28**(8), 1609–1621 (2022). https://doi.org/10.1108/RPJ-11-2021-0325
23. L. Thijs, M.L.M. Sistiaga, R. Wauthle, Q. Xie, J.-P. Kruth, J. Van Humbeeck, Strong morphological and crystallographic texture and resulting yield strength anisotropy in selective laser melted tantalum. Acta Mater. **61**(12), 4657–4668 (2013). https://doi.org/10.1016/j.actamat.2013.04.036
24. F. Trevisan, F. Calignano, M. Lorusso, J. Pakkanen, A. Aversa, E.P. Ambrosio, D. Manfredi, On the selective laser melting (SLM) of the AlSi10Mg alloy: process, microstructure, and mechanical properties. Materials **10**(1), 76 (2017). https://doi.org/10.3390/ma10010076